PNAS RESEARCH ARTICLE | CELL BIOLOGY OPEN ACCESS

Genome-wide CRISPR screens in spheroid culture reveal that the tumor suppressor LKB1 inhibits growth via the PIKFYVE lipid kinase

John R. Ferrarone[a,b,1], Jerin Thomas[a,2], Arun M. Unni[a], Yuxiang Zheng[a,3], Michal J. Nagiec[a,c], Eric E. Gardner[a], Oksana Mashadova[a,4], Kate Li[a], Nikos Koundouros[a,c], Antonino Montalbano[d,e,5], Meer Mustafa[d,e,6], Lewis C. Cantley[a,f,3], John Blenis[a,c], Neville E. Sanjana[d,e], and Harold Varmus[a,f,1]

Contributed by Harold Varmus; received February 22, 2024; accepted April 19, 2024; reviewed by Daniel A. Haber and Frank McCormick

The tumor suppressor LKB1 is a serine/threonine protein kinase that is frequently mutated in human lung adenocarcinoma (LUAD). LKB1 regulates a complex signaling network that is known to control cell polarity and metabolism; however, the pathways that mediate the tumor-suppressive activity of LKB1 are incompletely defined. To identify mechanisms of LKB1-mediated growth suppression, we developed a spheroid-based cell culture assay to study LKB1-dependent growth. We then performed genome-wide CRISPR screens in spheroidal culture and found that LKB1 suppresses growth, in part, by activating the PIKFYVE lipid kinase. Finally, we used chemical inhibitors and a pH-sensitive reporter to determine that LKB1 impairs growth by promoting the internalization of wild-type EGFR in a PIKFYVE-dependent manner.

LKB1 | STK11 | PIKFYVE | EGFR

Significance

Liver Kinase B1 (LKB1) is a tumor suppressor that is recurrently altered in lung adenocarcinoma, and mechanisms of LKB1-dependent growth suppression are incompletely understood. In this study, we used genome-wide CRISPR screens in spheroid culture to determine that LKB1 impairs growth via activation of the PIKFYVE lipid kinase. Furthermore, we determined that LKB1 promotes the internalization of Epidermal Growth Factor Receptor (EGFR) in a PIKFYVE-dependent manner.

The tumor suppressor gene *LKB1* (*STK11*) encodes a serine/threonine protein kinase that is inactivated in several types of human cancers, including up to 30% of lung adenocarcinomas (LUAD) (1). Tumors with inactivating mutations in *LKB1* are less responsive to both chemo- and immunotherapy, compared to tumors with wild-type (WT) *LKB1* (2). At present, it is unclear how alterations in *LKB1* promote tumorigenesis. Two studies using mouse models of lung cancer determined that the salt-inducible kinases (SIKs) are required for LKB1-dependent tumor suppression (3, 4). Downstream of the SIKs, the Cyclic AMP-responsive element binding protein (CREB)-regulated transcriptional coactivators (CRTCs) may play a role in inhibiting growth (3); however, it is unclear whether the CRTCs specifically mediate the tumor-suppressive effects of LKB1 or whether they are essential for tumor growth in general.

To determine the mechanisms of LKB1-mediated growth control, we developed a spheroid-based cell culture assay that recapitulated the growth-suppressive effects of LKB1 observed in animal models. We then conducted genome-wide loss-of-function CRISPR screens in spheroid culture and found that LKB1 opposes growth by activating the PIKFYVE lipid kinase. Further, we have determined that activation of PIKFYVE results in the internalization of WT EGFR and that EGFR is functionally important in LKB1-dependent suppression of growth.

Results

Expression of *LKB1* Limits Growth of *LKB1*-Null LUAD Lines in Spheroid Culture, But Not in Two-Dimensional (2D) Culture. To interrogate the function of LKB1 as a tumor suppressor, we used a retroviral vector to express WT *LKB1* stably in an *LKB1*-null human LUAD line (A549, *SI Appendix*, Fig. S1*A*). As expected, expression of *LKB1* led to a marked reduction in the growth of this line as subcutaneous xenografts in mice, compared to *LKB1*-null control cells containing an empty vector (EV) (Fig. 1*A*). However, the expression of *LKB1* had no effect on the growth of this line in 2D culture (Fig. 1*B*).

We then evaluated LKB1-dependent growth using a spheroid-based cell culture method. When A549 cells were grown as spheroids in a matrix formed from methylcellulose, reintroduction of *LKB1* dramatically reduced spheroid growth, relative to the *LKB1*-null condition (Fig. 1 *C* and *D*). We also determined that the kinase activity of LKB1 is required for growth suppression by expressing *LKB1-K78I* (5), a kinase-inactive (KI) version of *LKB1* (*SI Appendix*, Fig. S1*B*), which had no effect on growth in either 2D or spheroid culture (*SI Appendix*, Fig. S1 *C* and *D*). In agreement with the findings in mouse models (3, 4), the knockout of *SIK1* and *SIK3* with CRISPR/Cas9, or the treatment of spheroids with YKL-05-099 (6), a small molecule inhibitor of the SIKs, led to complete restoration of the growth of spheroids with *LKB1*, while having minimal effect on the growth of *LKB1*-null spheroids (Fig. 1 *E* and *F*). We also expressed WT *LKB1* in two additional *LKB1*-null LUAD lines (H2030 and

Reviewers: D.A.H., Massachusetts General Hospital; and F.M., University of California San Francisco.

Competing interest statement: H.V. is a member of the scientific advisory boards (SABs) for Dragonfly Therapeutics and Surrozen. N.E.S. is an advisor of Vertex and Qiagen and is a co-founder and advisor of OverT Bio. L.C.C. is a co-founder of Faeth Therapeutics, Volastra Therapeutics, and Larkspur Biosciences and is a member of their SABs. L.C.C. is also a co-founder of Agios Pharmaceuticals and is a former member of its SAB and board of directors. M.M. holds stock in 23andMe, Inc. All other authors declare no potential conflicts of interest.

[1]To whom correspondence may be addressed. Email: jrf9008@med.cornell.edu or varmus@med.cornell.edu.

[2]Present address: Donald and Barbara Zucker School of Medicine at Hofstra University, Hempstead, NY 11549.

[3]Present address: Department of Cell Biology, Harvard Medical School, Boston, MA 02215.

[4]Present address: Regeneron Pharmaceuticals, Tarrytown, NY 10591.

[5]Present address: Sana Biotechnology, Inc., Seattle, WA 98102.

[6]Present address: 23andMe, Inc., South San Francisco, CA 94080.

This article contains supporting information online at https://www.pnas.org/lookup/suppl/doi:10.1073/pnas.2403685121/-/DCSupplemental.

Published May 14, 2024.

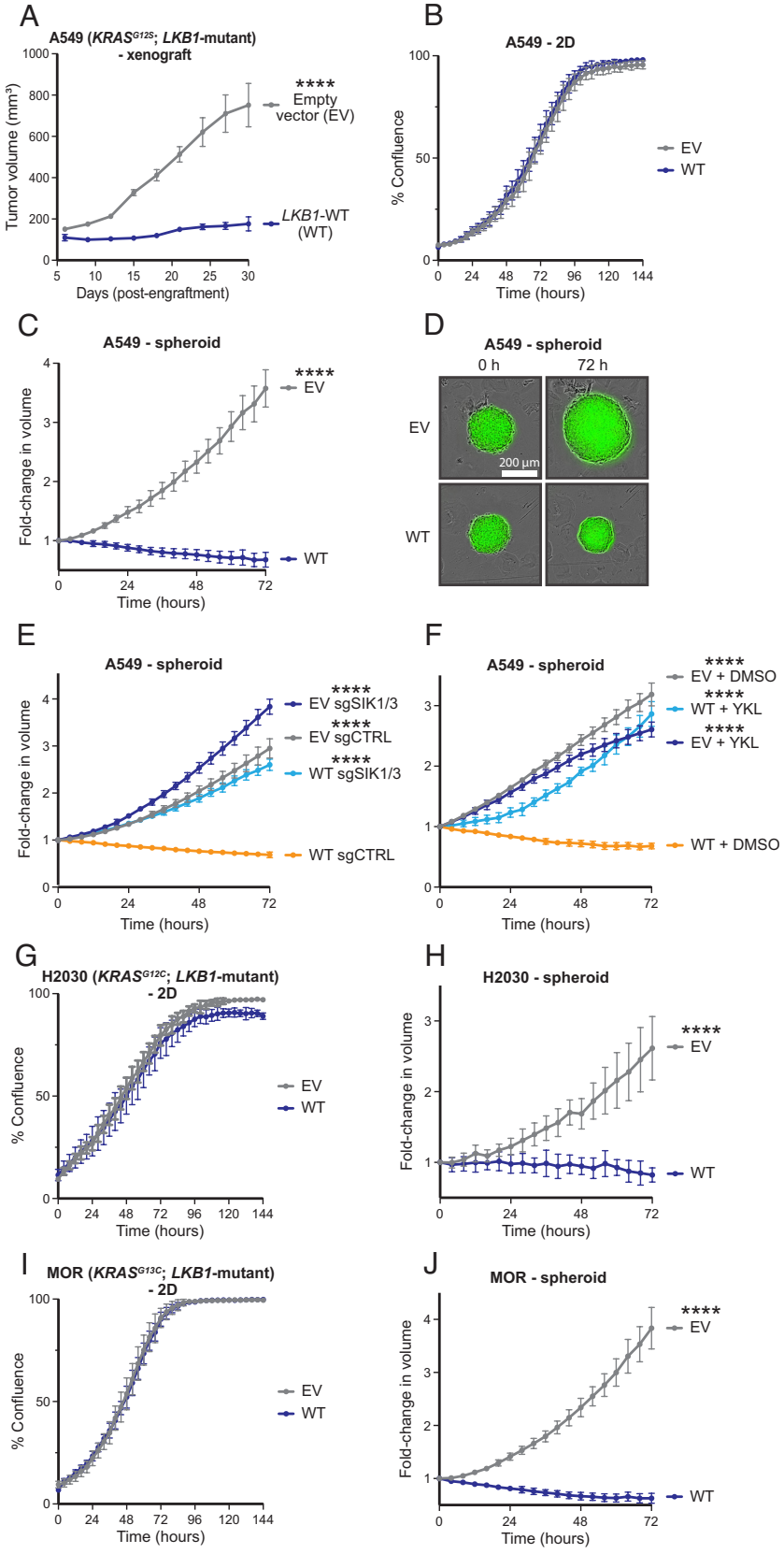

Fig. 1. Expression of *LKB1* limits growth of *LKB1*-null human LUAD lines in spheroid culture, but not in 2D culture. (*A*) Growth of A549 cells, which contain an EV, leaving the cells *LKB1*-null, or a vector expressing WT *LKB1*, as xenografts in the flanks of athymic mice. Tumor volume was measured every 3 d. Error bars indicate the SEM. n = 5. (*B*) Growth of A549 EV and WT cells in 2D culture. (*C* and *D*) Growth of A549 EV and WT cells in spheroid culture. Growth of the spheroids over 72 h is shown in panel (*C*), and representative images of the spheroids are shown in panel (*D*). (*E*) Spheroid growth of A549 EV and WT cells containing a control guide RNA (sgCTRL) or sgRNAs against *SIK1* and *SIK3*. (*F*) Spheroid growth of A549 EV and WT cells treated with dimethylsulfoxide (DMSO) or 2,000 nM of the SIK inhibitor YKL-05-099 (YKL). (*G–J*) Growth of H2030 and MOR EV and WT cells in 2D and spheroid culture. Growth measurements were obtained every 4 h using an Incucyte S3 live cell imager. For the spheroid culture experiments, growth is expressed as the fold-change in the volume of each spheroid. For the 2D culture experiments, growth is expressed as the percentage of the imaging field that is occupied by cells (i.e., % confluence). Error bars indicate SD. n = 3 to 6. **** indicates $P < 0.0001$. *P*-values indicate pairwise statistical comparisons to "WT sgCTRL" or "WT + DMSO" in panels (*E* and *F*).

MOR; *SI Appendix*, Fig. S1 *E* and *F*) and confirmed that LKB1 limited the growth of these lines as spheroids, but had no effect in 2D culture (Fig. 1 *G–J*). These data suggest that spheroid-based cell culture recapitulates the tumor-suppressive function of LKB1, as we observed with the subcutaneous xenografts.

We then attempted to recapitulate the tumor-suppressive activity of LKB1 in 2D culture by modulating the levels of nutrients in the media. Since the withdrawal of glucose in 2D culture led to activation of LKB1-mediated signaling (as measured by phosphorylation of AMPKα and ULK1) only in cells with WT *LKB1* (*SI Appendix*,

Fig. S2*A*), we reasoned that *LKB1*-expressing cells may exhibit reduced proliferation only under low glucose. However, reducing the levels of glucose, amino acids, or serum in the culture media had similar inhibitory effects on the growth of *LKB1*-null and -WT cells in 2D culture (*SI Appendix*, Fig. S2 *B–D*). Additionally, we tested the growth of these cells on plates with physiologic levels of surface tension, since mechanical forces can influence the activity of growth-promoting pathways (7). However, this also did not lead to a selective reduction in the growth of *LKB1*-WT cells (*SI Appendix*, Fig. S2*E*). Thus, these differences in nutrient availability or surface tension do not account for LKB1-dependent discrepancies in growth between 2D and spheroid culture.

LKB1 Suppresses the Activity of Oncogenic Signaling Pathways in Spheroid Culture, But Not in 2D Culture. To explain the differences in the effect of LKB1 on the growth of LUAD cells in 2D and spheroid culture, we evaluated the phosphoproteome of *LKB1*-null and -WT cells grown under these conditions. When cells were grown as spheroids, the abundance of phosphopeptides derived from proteins associated with the mitogen-activated protein kinase (MAPK) and the mammalian target of rapamycin complex 1 (mTORC1) signaling pathways was decreased in the *LKB1*-WT cells compared to *LKB1*-null cells (Fig. 2*A*). LKB1 is known to inhibit the mTORC1 pathway via activation of AMPK (1); however, LKB1 is not known to influence the activity of the MAPK pathway.

To identify changes in signaling that were specific to spheroid culture, we adjusted the relative phosphopeptide signal intensities (WT vs. EV) in spheroid culture to account for changes in the relative values of the same peptides in 2D culture. This revealed an even greater reduction in phosphopeptides corresponding to the mTORC1 pathway in the *LKB1*-WT cells relative to the null cells (Fig. 2*B*).

The protein kinases responsible for phosphorylation of many of the phosphopeptides identified in Fig. 2 *A* and *B* are not known. To make informed predictions about the relative activity of kinases in *LKB1*-null and -WT cells, we used a recently published program that predicts the activity of 303 serine and threonine kinases (8). Using normalized abundance of phosphopeptides from Fig. 2*B* as input for this program, the SIKs were among the kinases predicted to be most active in LKB1-containing cells in spheroid culture relative to 2D culture. In contrast, the activity of AKT1 kinase, a component of the mTORC1 pathway, was predicted to be the most suppressed under the same conditions (Fig. 2*C*). We then confirmed that LKB1 suppresses the activity of the mTORC1 pathway to a greater degree in spheroid culture than in 2D culture (Fig. 2*D*). We also noted that LKB1 suppressed the activity of the MAPK pathway to a greater extent in spheroid culture (Fig. 2*E*).

To assess whether the changes in the AKT1-mTORC1 pathway were functionally significant with respect to growth, we used lentiviral vectors to introduce constitutively active versions of *PIK3CA* (*PIK3CA-E545K*) or *AKT1* [myristoylated *AKT1* (*myrAKT1*)] in *LKB1*-null and -WT cells (*Materials and Methods*). The introduction of *PIK3CA-E545K* or *myrAKT1* partially restored the growth of spheroids with WT *LKB1*, but did not increase the growth rate of *LKB1*-null spheroids (Fig. 2*F*). Since activating mutations in the PI3K-AKT-mTORC1 pathway are known to drive tumor growth (9), these results suggest that inhibition of this pathway partially accounts for the tumor-suppressive activity of LKB1.

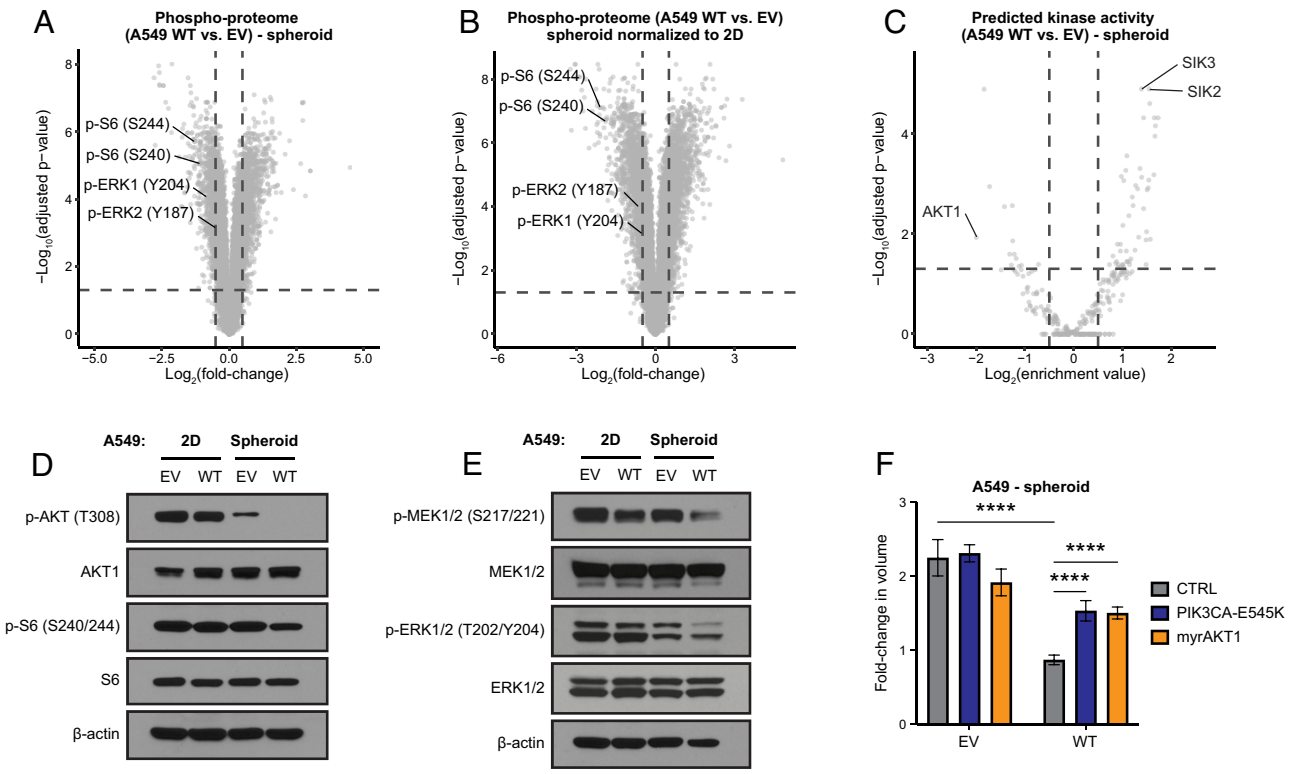

Fig. 2. LKB1 suppresses the activity of the mTORC1 and MAPK pathways in spheroid culture, but not 2D culture. (*A*) Relative abundance [expressed as $\log_2$(fold-change)] of phosphorylated peptides in A549 WT spheroids relative to EV spheroids. (*B*) A comparison of the relative phosphopeptide signal intensities (WT vs. EV) in spheroid culture after adjusting the fold-change values to account for changes in the relative abundance of the same peptides in 2D culture. In (*A* and *B*), phosphopeptides that correspond to proteins in the MAPK and mTORC1 pathways are labeled in black. (*C*) The predicted activity of serine and threonine kinases in WT spheroids relative to EV spheroids. (*D* and *E*) Levels of proteins phosphorylated in the mTORC1 (*D*) and MAPK (*E*) pathways in EV and WT cells, in 2D and spheroid culture. (*F*) Growth of A549 EV and WT spheroids transduced with an empty lentiviral vector (CTRL) or vectors that express *PIK3CA-E545K* or myristoylated *AKT1* (*myrAKT1*) after 72 h in culture. Error bars indicate SD. n = 3 to 6. **** indicates $P < 0.0001$.

Genome-Wide, Loss-of-Function CRISPR Screens in Spheroid Culture Identify Genes Required For LKB1-Mediated Tumor Suppression. Having established a system to study the tumor-suppressive effects of LKB1, we performed genome-wide CRISPR screens to identify genetic knockouts that enhanced the growth of A549 cells that express WT *LKB1* (WT) in spheroid culture. As controls, parallel screens were performed in spheroid cultures of *LKB1*-null A549 cells and in 2D cultures of A549 cells that were *LKB1*-null or that expressed *LKB1*.

To induce genetic knockouts using CRISPR/Cas9, we transduced *LKB1*-null or WT cells with a lentivirus vector carrying the TKOv3 (Toronto Knockout version 3) genome-wide CRISPR knockout library (10) (Fig. 3*A*). Following selection of infected cells with puromycin, cells were propagated in either 2D or spheroid culture. Genomic DNA was extracted from cells after 21 d in culture and then sequenced to determine the changes in the abundance of DNA sequences encoding single guide RNAs (sgRNAs) over the course of the experiment.

Strikingly, in the spheroid-based CRISPR screen in cells expressing *LKB1*, we noted a selective enrichment of DNA encoding sgRNAs that correspond to tumor suppressor genes that regulate growth factor receptors (the tyrosine phosphatase *PTPN12*), the Hippo pathway (*NF2*), and the mTORC1 pathway (*PTEN*, *TSC1*, and *TSC2*) (all shown in blue in Fig. 3*B*). Moreover, such enrichment was not observed in cells grown in 2D culture (Fig. 3*C*). Additionally, a Kyoto Encyclopedia of Genes and Genomes (KEGG) pathway analysis of the sgRNAs that were selectively enriched in *LKB1*-WT spheroids highlighted the ErbB, Hippo, and mTORC1 pathways (Fig. 3*D*). These findings imply that activation of these pathways may restore the growth of *LKB1*-expressing spheroids. These results are consistent with a prior study (12), which showed that LKB1 suppresses growth through the Hippo pathway. Our results also suggest that the LKB1-mediated changes in signaling in the MAPK and mTORC1 pathways (Fig. 2 *D* and *E*) may be functionally significant.

Of greater interest, we also observed an enrichment of sgRNAs corresponding to two genes involved in the regulation of 5′ phosphoinositides: *VAC14* and *FIG4* (shown in red in Fig. 3*B*). *VAC14* codes for a scaffold protein and *FIG4* encodes a 5′ phosphoinositide phosphatase that form a complex with PIKFYVE (Fig. 3*E*)—a 5′ phosphoinositide kinase (also known as phosphatidylinositol-3-phosphate 5-kinase type III or PIPKIII) (11). Together, this complex regulates the synthesis and turnover of phosphatidylinositol 3,5-bisphosphate (13–16) but has not been previously implicated in tumor suppression. The PIKFYVE complex also regulates endosomal trafficking (17), which is associated with one of the processes highlighted by the pathway analysis (endocytosis; Fig. 3*D*). Closer inspection of the results of the CRISPR screen showed that most of the individual sgRNAs for these genes were enriched in the *LKB1*-WT spheroids and either depleted or unchanged in spheroids lacking LKB1 (Fig. 3 *F* and *G*). In a replicate of these screens, DNA encoding sgRNAs against *VAC14* was again enriched in *LKB1*-WT cells grown in spheroid culture (*SI Appendix*, Fig. S3*A*).

LKB1 Mediates Growth Suppression through the PIKFYVE Complex. Next, we individually knocked out *FIG4* or *VAC14* in the A549 and MOR LUAD lines using multiple sgRNAs (*SI Appendix*, Fig. S3 *B–E*). We then confirmed that knockout of these genes modestly increased the growth of spheroids with WT *LKB1* (*SI Appendix*, Fig. S3 *F–I*) in a 3-d assay (as compared to the pooled screen, which was carried out over 21 d).

Although DNA encoding sgRNAs against *PIKFYVE* was not enriched in the CRISPR screen of spheroids with *LKB1*-WT, we also tested whether PIKFYVE mediates growth suppression, since *FIG4* and VAC14 are both known to regulate the activity of PIKFYVE (11).

We initially attempted to knock out (KO) *PIKFYVE* with CRISPR/Cas9, but we found that none of the four sgRNAs that we tested reduced PIKFYVE protein levels. As an alternative approach, we used the PIKFYVE inhibitor apilimod (API) (18) to ask whether the enzymatic activity of PIKFYVE affects spheroid growth. We found that apilimod clearly enhanced the growth of spheroids containing WT *LKB1*, but had no effect on the growth of spheroids lacking LKB1 (Fig. 3*H*). To verify that apilimod was acting on its known target, we expressed a mutant version of *PIKFYVE* [N1939K, which is resistant to the inhibitory effect of apilimod (19)] in the *LKB1*-null and -WT cells. In spheroids with *LKB1*, this PIKFYVE mutant impaired the restoration of growth in the presence of apilimod (Fig. 3*I*). Furthermore, the PIKFYVE mutant had no effect on the growth of the *LKB1*-null spheroids (Fig. 3*J*), which suggests that LKB1 is required for the activation of PIKFYVE. We also confirmed that apilimod restores the growth of spheroids with WT *LKB1* derived from two other LUAD lines (H2030 and MOR; Fig. 3 *K* and *L*).

To assess for clinical evidence of a relationship between LKB1 and the PIKFYVE complex, we compared mRNA levels for *PIKFYVE*, *FIG4*, and *VAC14* in *LKB1*-WT and -mutant LUAD tumors from the TCGA dataset (20). We found that while *LKB1* mutational status had no effect on *PIKFYVE* mRNA levels, the mean levels of mRNA for *FIG4* and *VAC14* were significantly lower in the *LKB1*-mutant group compared to the *LKB1*-WT group (*SI Appendix*, Fig. S3 *J–L*).

Additionally, we used apilimod to treat three LUAD lines that harbor endogenous WT *LKB1* (Calu-1, H1792, and SW1573). We found that apilimod augmented the growth of all three lines as spheroids (*SI Appendix*, Fig. S4 *A–C*), indicating that PIKFYVE also behaves as a tumor suppressor in cells with endogenous WT *LKB1*.

To gauge whether LKB1 directly or indirectly mediates the activation of the PIKFYVE complex, we used a program (described above) (8) to predict the kinases for all previously reported phosphoserine or -threonine residues on the PIKFYVE complex. Through this approach, we identified numerous sites on PIKFYVE (a 240 kDa protein) that were predicted to be phosphorylation targets of the Adenosine monophosphate-activated protein kinase (AMPK)-related kinases (*SI Appendix*, Fig. S5*A*)—a family of closely related enzymes that are directly activated by LKB1, including the SIKs (1). Closer inspection of these results revealed 6 sites on PIKFYVE that were predicted to be substrates of the SIKs (*SI Appendix*, Fig. S5*B*). One of these sites, Ser307, was previously confirmed to be a target of AMPK (21), and phosphorylation was shown to stimulate the lipid kinase activity of PIKFYVE (21). Given that AMPK and the SIKs are known to share substrates (1), it is possible that LKB1 may activate PIKFYVE indirectly through the SIKs, as well as through AMPK.

LKB1 Promotes the Internalization of EGFR through PIKFYVE. Since PIKFYVE is known to regulate the degradation of growth factor receptors (including EGFR and Mesenchymal Epithelial Transition (MET)) (22, 23), and given that our CRISPR screen highlighted genes involved in ErbB signaling as potential mediators of LKB1-dependent tumor suppression, we investigated whether LKB1 influenced the internalization of EGFR through PIKFYVE. To do this, we used a pH-sensitive dye that is conjugated to EGF (pHrodo EGF) and fluoresces when exposed to the acidic environments of the endosomal and lysosomal compartments to indicate that EGF-EGFR complexes have been internalized (24). When we provided *LKB1*-null and -WT spheroids of A549 cells with pHrodo EGF, we noted that fluorescence signal intensity

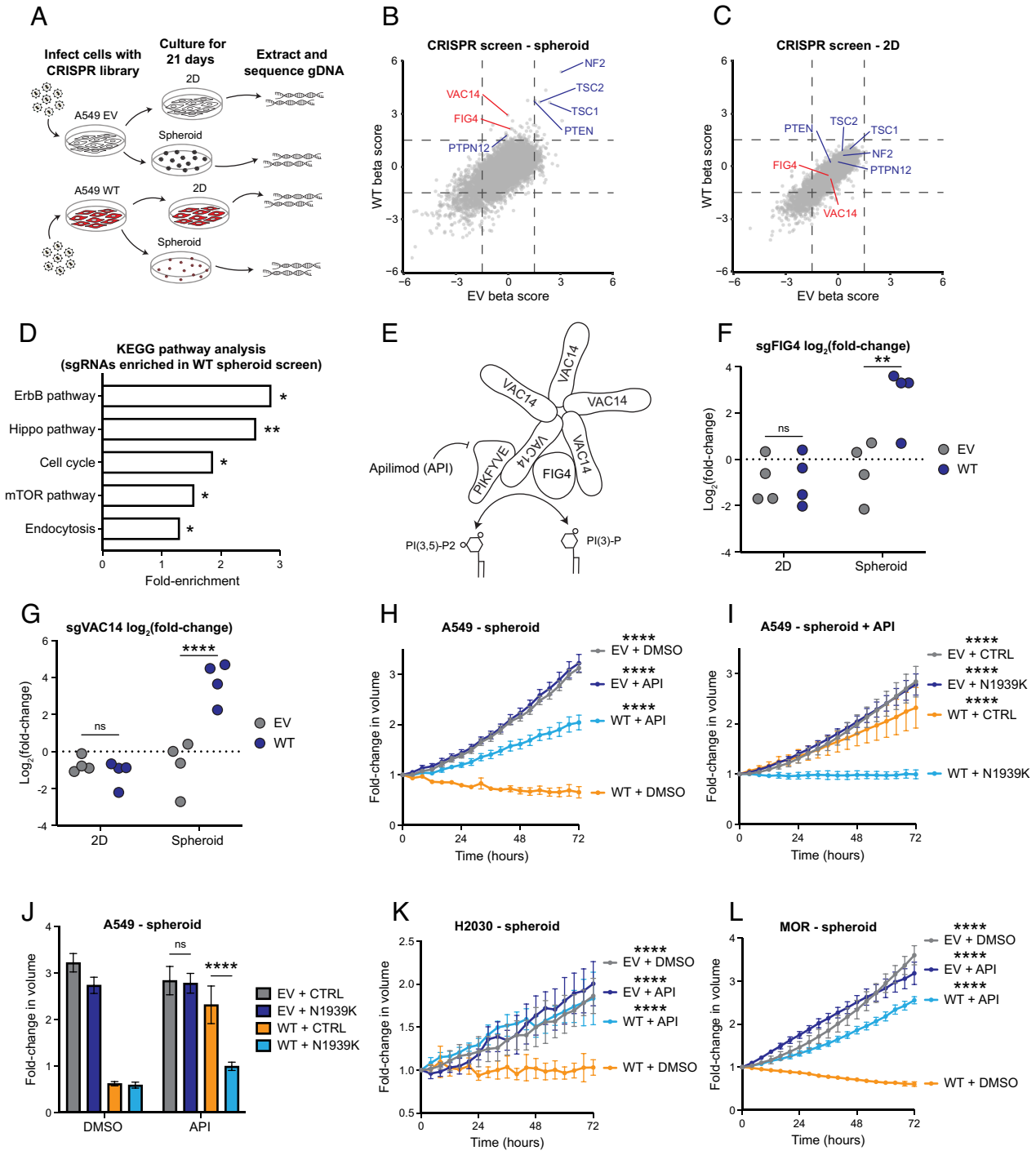

Fig. 3. Genome-wide CRISPR screens identify the PIKFYVE lipid kinase complex as a mediator of LKB1-dependent tumor suppression. (*A*) Schematic representation of the CRISPR screen experiment. (*B* and *C*) Beta score plot of DNAs encoding sgRNAs from cultures of A549 EV and WT cells transduced with a genome-wide CRISPR library and grown in spheroid (*B*) or 2D (*C*) culture. Members of the PIKFYVE lipid kinase complex are labeled in red lettering. Known tumor suppressor genes are labeled in blue lettering. Beta score is a weighted score of the $\log_2$(fold-change) values of all sgRNAs for a given gene. (*D*) An enrichment analysis of the sgRNAs that were enriched in the WT spheroids (beta score >1) but not in the EV spheroids (beta score < 1). (*E*) A representation of the structure of the PIKFYVE lipid kinase complex (11). (*F* and *G*) $\log_2$(fold-change) values of individual sgRNAs corresponding to *FIG4* (*E*) or *VAC14* (*F*) in A549 EV and WT cells grown in 2D or spheroid culture. (*H*) Growth of A549 EV and WT spheroids treated with DMSO or 100 nM of the PIKFYVE inhibitor apilimod (API). (*I* and *J*) Growth of A549 EV and WT spheroids transduced with an empty lentiviral vector (CTRL) or a vector that expresses a PIKFYVE mutant (N1939K) that is API resistant and treated with DMSO or API 100 nM. The growth curve in (*I*) shows the growth of these spheroids in API over a 72-h period, whereas the bar graph in (*J*) depicts the fold-change in the volume of the spheroids after 72 h in culture in DMSO or API. (*K* and *L*) Growth of EV and WT spheroids derived from H2030 (*K*) or MOR (*L*) in the presence of DMSO or API. Error bars indicate SD. n = 3 to 6. *, **, and **** indicate $P < 0.05$, 0.01, and 0.0001, respectively. ns, nonsignificant. *P*-values indicate pairwise statistical comparisons to "WT + DMSO" in panels (*H*, *K*, and *L*) and "WT + N1939K" in panel (*I*).

was markedly higher in the *LKB1*-WT spheroids relative to the *LKB1*-null spheroids (Fig. 4 *A* and *B*). Pretreatment of these spheroids with apilimod (a PIKFYVE inhibitor), YKL-05-099 (a SIK inhibitor), or chloroquine (CQ) (an inhibitor of endocytosis) reduced the fluorescence of *LKB1*-WT spheroids fed with pHrodo EGF (Fig. 4*C*). Additionally, we asked whether loss of LKB1 in cells with endogenous WT LKB1 would result in a decrease in the internalization of EGFR. To do this, we used CRISPR/

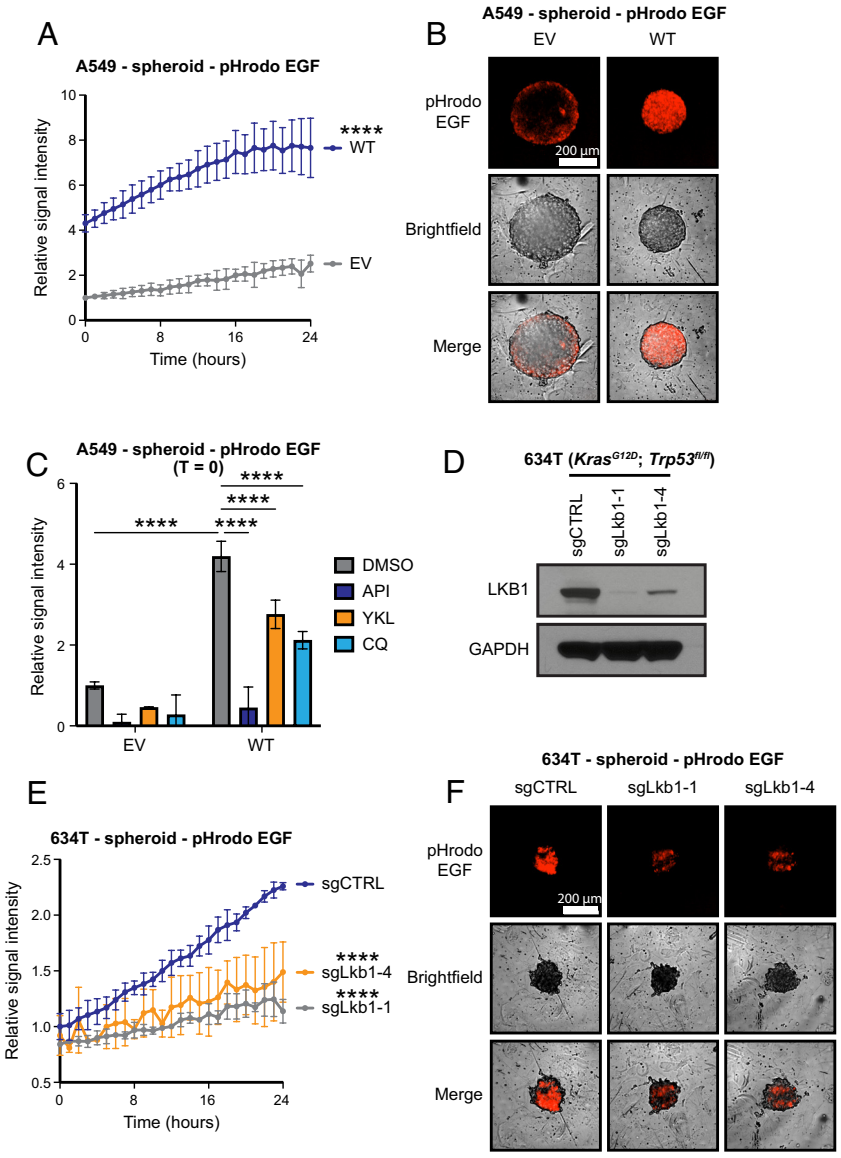

Fig. 4. LKB1 promotes the endocytosis of EGFR through PIKFYVE. (*A*) Relative signal intensity of A549 EV and WT spheroids treated with a pH-sensitive reporter that indicates the internalization of EGFR (pHrodo EGF). (*B*) Representative images of EV and WT spheroids treated with pHrodo EGF. (*C*) Relative signal intensity of EV and WT spheroids treated with DMSO, API 100 nM, YLK 2,000 nM, or chloroquine (CQ) 10 µM and pHrodo EGF. (*D*) Lkb1 protein levels in a $Kras^{G12D}$;$Trp53^{fl/fl}$ mouse lung tumor line (634T) containing a control guide RNA (sgCTRL) or guide RNAs targeting *Lkb1* (sgLkb1) (*E*) Relative signal intensity of 634T spheroids containing sgCTRL or sgLkb1 that were treated with pHrodo EGF. (*F*) Representative images of 634T sgCTRL and sgLkb1 spheroids treated with pHrodo EGF. Error bars indicate SD. n = 3 to 4. **** indicates $P < 0.0001$. For experiments with 634T cells, *P*-values indicate pairwise statistical comparisons to "sgCTRL."

Cas9 to KO *Lkb1* in a $Kras^{G12D}$;$Trp53^{fl/fl}$ mouse lung tumor line (634T, Fig. 4*D*) (25). When spheroids derived from these cells were treated with pHrodo EGF, we noted a marked decrease in fluorescence of the spheroids with *Lkb1*-KO compared to the *Lkb1*-intact controls (Fig. 4 *E* and *F*). Altogether, these results suggest that LKB1 promotes the endocytosis of EGFR through both the SIKs and PIKFYVE.

To determine whether LKB1 influences the endocytosis of proteins and extracellular molecules more broadly, we evaluated the effect of LKB1 on the uptake of transferrin or dextran labeled with pHrodo. Similar to our findings with EGFR, we found that LKB1 promoted the endocytosis of transferrin and dextran. This effect was again reversed when the spheroids were pretreated with apilimod, with a SIK inhibitor, or with CQ (*SI Appendix*, Fig. S6 *A–F*). Furthermore, the knockout of *Lkb1* in 634T spheroids reduced the uptake of both transferrin and dextran (*SI Appendix*, Fig. S6 *G–J*). Therefore, LKB1 promotes the endocytosis of cell surface receptors and extracellular polysaccharides in a SIK- and PIKFYVE-dependent manner.

LKB1 Impairs Growth through Regulation of EGFR. We then sought to determine whether LKB1-mediated growth suppression could be attributed to regulation of EGFR. To gauge whether this was likely, we first evaluated the rate of co-occurrence of mutations in *LKB1* and *EGFR*, since mutational patterns in tumor sequencing data can reveal pathways that cooperate or antagonize each other in tumorigenesis (26). Upon our analysis of three sequencing studies of human LUAD tumors (27), we found that mutations in *LKB1* and *EGFR* did not co-occur in any tumors (Fig. 5 *A* and *B*). This suggests that mutations in *LKB1* and *EGFR* are either functionally redundant or toxic when they co-occur, due to their regulatory effects on a common pathway. To determine whether mutations in *EGFR* and *LKB1* are functionally redundant, we used CRISPR/Cas9 to knockout *LKB1* in two *EGFR*-mutant/*LKB1*-WT LUAD lines (PC9 and H1975) (*SI Appendix*, Fig. S7 *A* and *B*). We then tested the growth of these cells in spheroid culture and found that loss of LKB1 had no effect on growth (*SI Appendix*, Fig S7 *C* and *E*). Additionally, treatment of parental PC9 and H1975 cells with apilimod did not decrease the rate of growth in spheroid culture (*SI Appendix*, Fig S7 *D* and *F*). Together, these results suggest that alterations in *EGFR* and the LKB1-PIKFYVE pathway are functionally redundant.

Since a previous study showed that LKB1 influences the phosphorylation of not only EGFR, but also MET, HER2, and FGFR4 (28), we assessed whether alterations in these other receptors were mutually exclusive with mutations in *LKB1*. We found that

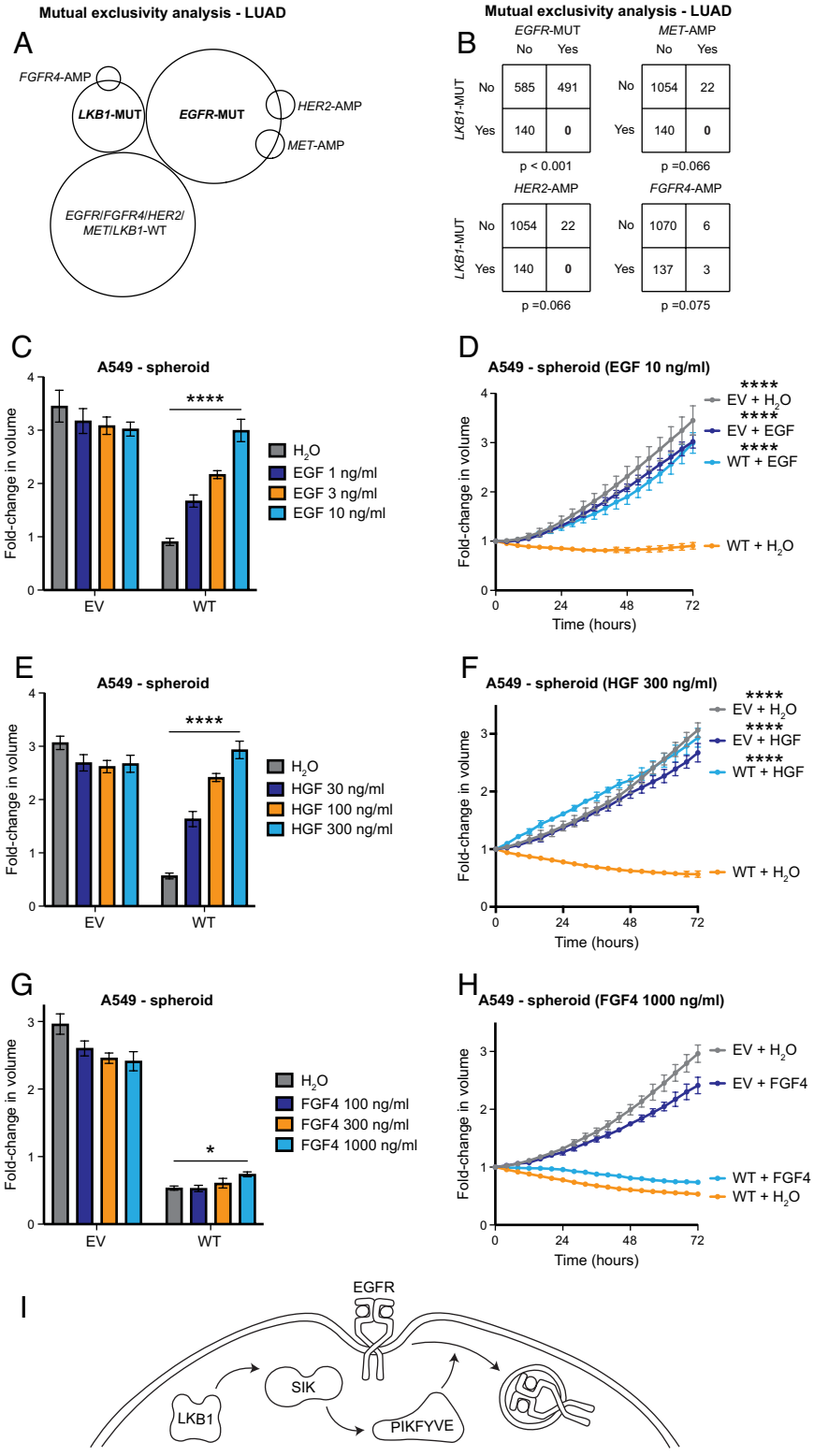

Fig. 5. LKB1 suppresses growth by antagonizing the function of growth factor receptors. (*A* and *B*) Mutual exclusivity analysis of mutations in *LKB1* and *EGFR* and amplifications of *HER2*, *FGFR4*, and *MET* in human LUAD tumors. (*C*–*H*) Growth of A549 EV and WT spheroids treated with H_2O, EGF, HGF, or FGF4 at 72 h in culture and in different doses of growth factors (*C*, *E*, and *G*), or over a period of 72 h in H_2O or growth factors at the indicated doses (*D*, *F*, and *H*). (*I*) A model of LKB1-mediated growth suppression. Error bars indicate SD. n = 3 to 6. * and **** indicate $P < 0.05$ and 0.0001, respectively. *P*-values indicate pairwise statistical comparisons to "WT + H_2O" in panels (*D*, *F*, and *H*).

amplifications in *MET* and *HER2* did not co-occur with mutations in *LKB1*, whereas amplifications in *FGFR4* did co-occur with mutations in *LKB1* (Fig. 5*A*), but the frequencies at which these receptors were amplified were too small to determine whether the patterns were statistically significant (Fig. 5*B*). Importantly, the addition of EGF or HGF to the culture media fully restored the growth of spheroids with WT *LKB1* in a dose-dependent manner, while having no effect on spheroids lacking LKB1 (Fig. 5 *C*–*F*). In contrast, even high doses of FGF4 had minimal effect on the growth of spheroids with WT *LKB1* (Fig. 5 *G* and *H*). Taken as a whole, these findings suggest that LKB1 inhibits growth by reducing the availability of WT EGFR and possibly other growth factor receptors, such as MET, on the cell surface. Thus, we propose that LKB1 inhibits progrowth signaling by promoting the endocytosis of growth factor receptors via the SIKs and PIKFYVE (Fig. 5*I*).

Loss of *Lkb1* Sensitizes *Kras*-Mutant Mouse Lung Tumor Cells to Combined Inhibition of Egfr and Kras. Given that LKB1 may suppress growth by facilitating the internalization of EGFR, we

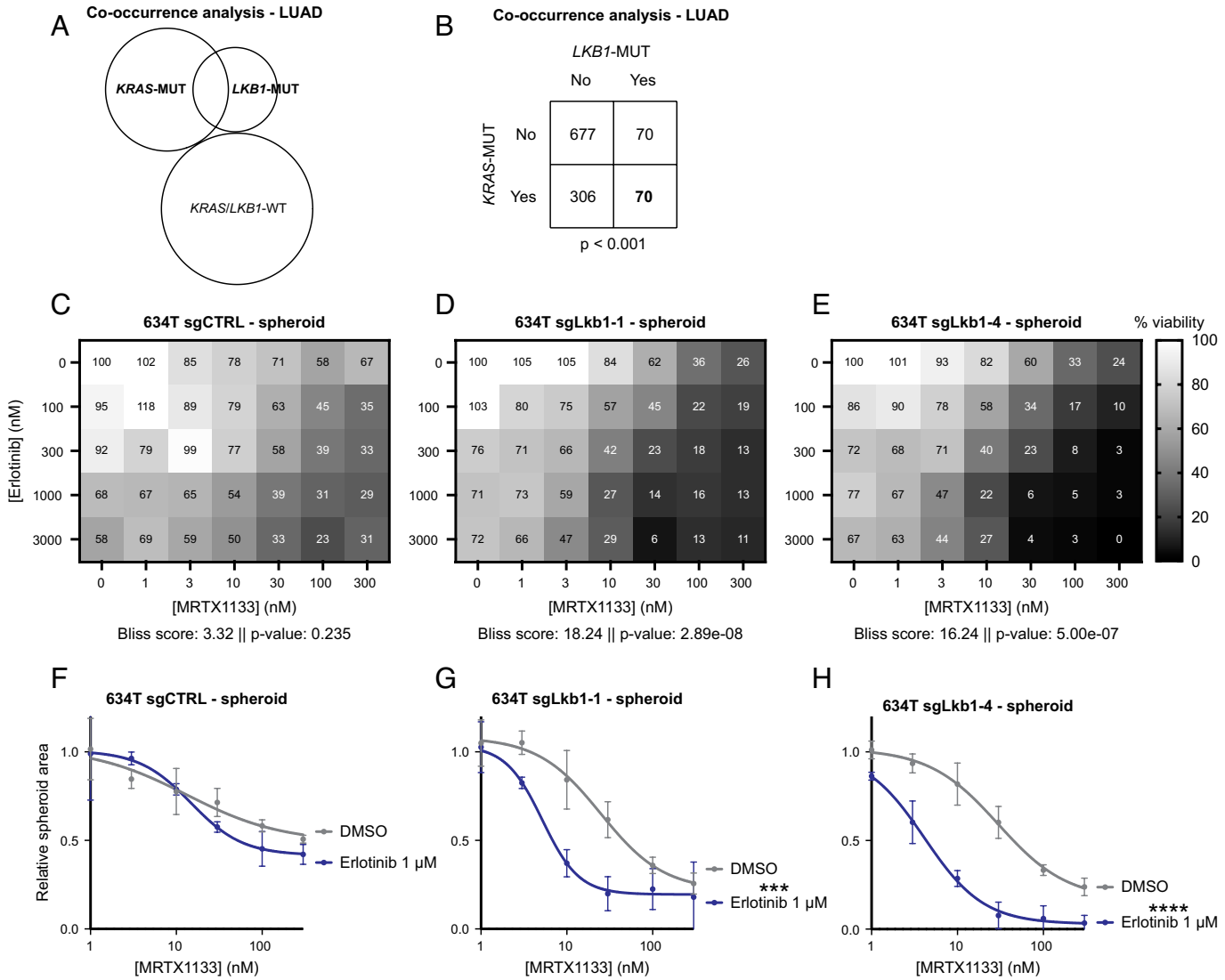

Fig. 6. Loss of *Lkb1* sensitizes *Kras*-mutant murine lung tumor cells to combined inhibition of Egfr and Kras. (*A* and *B*) Co-occurrence analysis of mutations in *LKB1* and *KRAS* in human LUAD tumors. (*C–E*) Dose–response matrices of 634T (*Kras*^{G12D}; *Trp53*$^{fl/fl}$) spheroids treated with erlotinib or the KRAS-G12D inhibitor MRTX1133 and containing sgCTRL (*C*) or sgRNAs against *Lkb1* (*D* and *E*). The number listed over each condition corresponds to the percent viability of each spheroid relative to untreated spheroids (as measured by total spheroid area). Each condition represents the average percent viability of 3 to 4 spheroids. Additionally, drug synergy (Bliss) scores and their associated *P*-values are indicated below each matrix. (*F–H*) Dose–response curves of MRTX1133 in 634T spheroids containing sgCTRL (*F*) or sgRNAs against *Lkb1* (*G* and *H*) in the presence or absence of erlotinib 1 μM. Error bars indicate SD. n = 3 to 4. *** and **** indicate $P < 0.0002$ and 0.0001, respectively.

wondered whether lung cancer cells with mutations in *LKB1* may be driven by WT EGFR. Prior studies have shown that WT EGFR can augment the activity of oncogenic KRAS (29, 30). Oncogenic mutations in *KRAS* occur in approximately 50% of LUADs that harbor mutations in *LKB1* (Fig. 6 *A* and *B*). Therefore, in *KRAS*-mutant tumors, loss of LKB1 could promote the activity of KRAS through an increase in the activity of WT EGFR. Thus, we asked whether inhibition of EGFR would increase the sensitivity of *KRAS*-mutant lung cancer cells to inhibition of oncogenic KRAS. To do this, we treated spheroids derived from control and *Lkb1*-knockout 634T cells (depicted in Fig. 4*D*) with various concentrations of the EGFR inhibitor erlotinib, along with the KRAS-G12D inhibitor MRTX1133 (31). We found that treatment of Lkb1-intact cells with erlotinib and MRTX1133 did not have a synergistic effect, as indicated by a drug synergy score (Bliss score = 3.32) (32) that did not meet statistical significance ($P = 0.235$) (Fig. 6*C*). However, in cells containing a knockout of *Lkb1*, the combination of erlotinib and MRTX1133 had a clear synergistic effect, as indicated by Bliss scores that were statistically significant (Fig. 6 *D* and *E*). This observation was especially evident when viewing the effect of erlotinib 1 μM on the sensitivity of these cells to a range of doses of MRTX1133. Erlotinib had minimal effects on the sensitivity of Lkb1-intact cells to the KRAS inhibitor (Fig. 6*F*), but the efficacy of MRTX1133 was increased in cells with a knockout of *Lkb1* (Fig. 6 *G* and *H*). These results are consistent with the idea that loss of LKB1 drives the growth of lung cancer cells through an increase in the activity of KRAS mediated by WT EGFR and further suggests that LKB1-dependent suppression of growth involves the regulation of EGFR.

Discussion

LKB1 controls a broad and incompletely defined signaling network, complicating efforts to identify the proteins responsible for the tumor-suppressive activity of LKB1—particularly those proteins positioned downstream of the SIKs. To address this challenge, we used an assay based in spheroid culture to study the tumor-suppressive function of LKB1. This allowed us to perform

an unbiased genome-wide CRISPR screen for genes required for growth suppression by LKB1. Additionally, the spheroid culture system enabled a detailed study of the function of LKB1 in human LUAD lines. The use of human cells is significant because LKB1-mediated signaling downstream of the SIKs is known to differ in some respects between mouse and human cells (33).

Our CRISPR screen identified two genes—*FIG4* and *VAC14*, both of which encode components of the PIKFYVE complex—as elements required for LKB1-mediated growth control. Moreover, chemical inhibition of PIKFYVE itself impaired growth suppression by LKB1. Since LKB1 is known to phosphorylate and activate PIKFYVE through AMPK—a kinase that is closely related to the SIKs—it is likely that LKB1-SIK may also activate the PIKFYVE complex through direct phosphorylation of PIKFYVE, as opposed to the other members of the complex, FIG4 and VAC14.

Additionally, we provide evidence that LKB1—through PIKFYVE—may broadly activate the endocytosis of cell surface receptors and extracellular nutrients. This action of LKB1-PIKFYVE results in the internalization of WT EGFR, which could impair growth by rendering a cell less responsive to the ligand for EGFR, EGF. Since LKB1 is generally thought to inhibit anabolic cellular processes when a cell is under nutrient stress (1), a global upregulation of endocytosis by LKB1-PIKFYVE may serve this end by decreasing the responsiveness of a cell to growth factors, in order to limit cell growth and proliferation when nutrients are scarce. LKB1 is also known to impair anabolic metabolism by inhibiting mTORC1 (1), a major driver of the synthesis of proteins, lipids, and nucleotides. Thus, regulation of anabolic metabolism by LKB1 may be attributed to its effects at the level of growth factor receptors, as well as mTORC1.

Endocytosis has been shown to play a role in increasing—as well as reducing—signaling from ligand-bound growth factor receptors (34). In the latter case, EGFR that has been endocytosed is delivered to the lysosome for degradation. However, in prostate cancer, signaling from internalized EGFR can be sustained via a p38-dependent mechanism, which impairs the degradation of EGFR (35). Thus, in the context of malignancy, the maintenance of signaling from endocytosed EGFR may require a reduction in the delivery of EGFR to the lysosome, which would increase the half-life of this receptor. Given that LKB1 has been shown to augment lysosomal activity through activation of AMPK (36), it is possible that mutations in *LKB1* may promote EGFR-mediated signaling through a decrease in both the internalization and degradation of EGFR.

We also note that PIKFYVE accounts for only part of the regulatory effect of LKB1 on EGFR. Prior studies have shown that LKB1 promotes the dephosphorylation of growth factor receptors, including EGFR, by activating protein tyrosine phosphatases, such as PTPN12 (28). Therefore, LKB1 may inhibit WT EGFR through at least two distinct mechanisms: by promoting PIKFYVE-dependent endocytosis of EGFR and by deactivating internalized EGFR via protein tyrosine phosphatases.

Finally, our findings demonstrate the power of spheroid culture to identify biological pathways that are not active in 2D culture. Furthermore, given that other tumor suppressors have been reported to suppress growth in three-dimensional culture, but not in 2D culture (37), our approach of combining genome-wide CRISPR with spheroid culture could be used to identify mechanisms of growth control by other poorly understood tumor suppressors.

Materials and Methods

Cell Lines and Culture Media. All LUAD cell lines (A549, Calu-1, H1792, H2030, MOR, and SW1573) used in this study were obtained from ATCC or Sigma-Aldrich (MOR only). The 634T cells were a generous gift from the laboratory of Kwok Wong (NYU). Cells were cultured in Roswell Park Memorial Institute (RPMI)-1640 (Corning 10-040-CV) supplemented with penicillin–streptomycin and 10% fetal bovine serum. Spheroids were grown in medium supplemented with methylcellulose (Thermo Fisher Scientific M352-500). To prepare 100 mL of methylcellulose-containing medium, 1.2 g of methylcellulose was autoclaved in a bottle containing a stir bar. One hundred ml of medium was warmed to 37 °C and then added to the methylcellulose. The methylcellulose medium was then shaken vigorously and allowed to dissolve at 4 °C overnight, with stirring. Cells were maintained at 37 °C in a humidified incubator containing 5% CO2. All cell lines (and their derivatives) were confirmed to be mycoplasma-free using the MycoAlert mycoplasma detection kit (Lonza LT07-218) at the beginning and upon completion of all experiments.

2D and Spheroid Growth Assays. 2D growth assays were performed by seeding 5,000 cells per well into flat-bottom 96-well plates (Corning 3603). For 2D growth assays in media with reduced nutrients or serum, 2,500 cells per well were seeded into flat-bottom 96-well plates. Twenty-four hours later, the cells were rinsed twice with phosphate-buffered saline (PBS), and then, medium containing variable levels of glucose, amino acids, or serum was added. Dialyzed FBS was used for all the experiments in which cells were grown with reduced levels of nutrients or serum. For 2D growth assays on plates with different levels of surface tension, 1.5×10^5 cells were seeded into 6-well CytoSoft plates (Advanced Biomatrix 5190). Images of these cells were taken every 4 h using an Incucyte Zoom or Incucyte S3 live cell imaging system.

Single spheroid growth assays were performed by seeding 100 cells per well (for H2030), 500 cells per well (for Calu-1, H1792, SW1573, and 634T cell lines), or 1,000 cells per well (for A549 and MOR cell lines) into low-attachment, V-bottom 96-well plates (S-bio MS-9096VZ) containing 100 μL of regular media per well. The plate was spun at 300 × g for 5 min and then placed in an incubator overnight. The following day, 80 μL of medium was slowly aspirated from each well, and then, 80 μL of methylcellulose-containing medium was layered on top of each spheroid. For all 96-well assays, a total of 100 μL of medium (with or without added methylcellulose) was used per well. Images of live cells were taken every 4 h using an Incucyte Zoom or Incucyte S3 live cell imaging system. The volume of an individual spheroid was derived from the total cross-sectional area of the spheroid. The start of each spheroid growth assay (T = 0 h) was approximately 8 h after the addition of methylcellulose. For all live cell imaging experiments, a minimum of three replicates were performed for each condition. Wells were excluded from analysis if the Incucyte failed to image a spheroid at any time point.

Spheroid Growth Assays with Inhibitors of EGFR and KRAS. Cells derived from the 634T line were seeded into low-attachment, V-bottom 96-well plates as described above. The following day, 80 μL of medium was slowly aspirated from each well, and then 80 μL of methylcellulose-containing medium was layered on top of each spheroid. Twenty-four hours after adding methylcellulose, erlotinib (MedChem Express HY-50896) and MRTX1133 (MedChem Express HY-134813) were diluted in RPMI and added to the spheroids. Plates were imaged in an Incucyte S3 live cell imaging system after 5 d of treatment. Green fluorescent protein (GFP) signal was used to determine the area of a spheroid, and the area of the spheroid was used a surrogate for the number of viable cells within a spheroid. SynergyFinderPlus (https://tangsoftwarelab.shinyapps.io/synergyfinder/) was used to calculate Bliss synergy scores of erlotinib and MRTX1133 in the cell lines derived from 634T.

Cloning and Retrovirus Preparation. Plasmids containing complementary DNAs (cDNAs) encoding WT and KI *LKB1* alleles were synthesized by Twist Biosciences. The alleles also contain mutations that confer resistance to CRISPR/Cas9 editing (without changing the amino acid sequence) with all the sgRNAs against *LKB1* in the TKOv3 CRISPR library (Addgene 125517, a gift from Jason Moffat). These alleles were then cloned into pBABE-GFP (Addgene 10668, a gift from William Hahn, Broad Institute) or pBABE-Hygro (Addgene 1765, a gift from Hartmut Land, University of Rochester) by first linearizing these backbones with EcoRI and then performing a Gibson assembly with NEBuilder HiFi DNA Assembly Master Mix (NEB E2621L). To generate the plasmid coding for PIKFYVE-N1939K, cDNA fragments for *PIKFYVE-N1939K* were synthesized by Twist Biosciences. These fragments were then cloned into pLV-EF1a-IRES-Puro (Addgene 85132, a gift from Tobias Meyer, Weill Cornell Medicine) by first linearizing the backbone with EcoRI and then performing a Gibson assembly. Plasmids coding for *PIK3CA-E545K* (Addgene 82881; a gift from Jesse Boehm (Broad Institute), Matthew

Meyerson (Dana Farber Cancer Institute), David Root (University of Colorado)) and *myrAKT1* (Addgene 64606, a gift from David Sabatini and Kris Wood, Duke) were purchased from Addgene, and the cDNAs encoding the *PIK3CA-E545K* and *myrAKT1* alleles were subcloned into pLV-EF1a-IRES-Puro via Gibson assembly. Retrovirus vectors were generated by cotransfecting the *LKB1*-containing plasmids with the pCMV-VSV-G packaging plasmid (Addgene 8454, a gift from Robert Weinberg, Massachusetts Institute of Technology) into GP2-293 cells (Takara 631458). Lentivirus was generated by transfecting the *PIKFYVE*-containing plasmid with the packaging plasmids pMD2.G and psPAX2 (Addgene 12259 and 12260, gifts from Didier Trono, École polytechnique fédérale de Lausanne) into 293FT cells (Invitrogen R70007) using Lipofectamine 3000 (Invitrogen L3000015). Media were changed 5h after transfection, and then, the supernatant was collected 48 h later.

Editing with CRISPR/Cas9 and Lentivirus Production. To KO a single gene, an sgRNA was cloned into the LentiCRISPRv2 plasmid (Addgene 52961, a gift from Feng Zhang, Broad Institute) or the LentiCRISPRv2-GFP plasmid (Addgene 82416, a gift from David Feldser, University of Pennsylvania). To knockout a second gene in the same line, an sgRNA was cloned into the LRT2B plasmid (Addgene 110854, a gift from Lukas Dow, Weill Cornell Medicine). Lentivirus was generated from these plasmids using the procedure described above.

The sgRNA sequences used in this study are as follows: sgCTRL, GTCTGTATTTC AGTCTGTGA and GGTTGGATAAGGCTTAGAAA (only as a control for the knockout of a second gene in the same line); sgSIK1, ATGGTCGTGACAGTACTCCA; sgSIK3, GTGCTTGCAGATCTGCTCCA; sgFIG4-2, AACCGCTCGAAATAAGCCCG; sgFIG4-4, TGATGGGAGAGCCAAACCTC; sgVAC14-1, AAAGCGGAAGGTGGCAGCGC; sgVAC14-2, GCCCACCTTGCCCAGTGCGA; sgLkb1-1, CCAGGCCGTCAATCAGCTGG; and sgLkb1-4, GAACAATGCCCTGGCTGTGT.

Inhibitors and Growth Factors. For all spheroid culture-based assays where inhibitors or growth factors were used, cells were seeded into medium containing the vehicle (DMSO or H_2O), inhibitor, or growth factor. The following day, media were aspirated and replaced with methylcellulose-containing media that also contained the vehicle, inhibitor, or growth factor. The vehicle concentration was 0.1% for all experiments. Inhibitors used in these experiments are as follows: YKL-05-099 (MedChem Express HY-101147), apilimod (MedChem Express HY-14644), and CQ (MedChem Express HY-17589A). Growth factors used in these experiments are as follows: EGF (PeproTech AF-100-15), FGF4 (PeproTech AF-100-31), and HGF (PeproTech 100-39H).

Mice and Xenografts. Animal procedures were performed with the approval of the Weill Cornell Medicine Institutional Animal Care and Use Committee (IACUC). Tumor volume was not allowed to exceed 1,000 mm^3. Prior to implantation, cells were resuspended in PBS and mixed 1:1 with Matrigel (Corning 356231). For the A549 xenograft experiment, 10^6 cells were injected into single flanks of 6-wk-old, female athymic mice (Envigo). Caliper measurements were performed every 3 d to monitor tumor growth.

Detection of Total and Phosphorylated Proteins. For western blot experiments, protein lysates were prepared in radioimmunoprecipitation assay (RIPA) buffer and quantified using a bicinchoninic acid (BCA) protein assay (Thermo Scientific 23225). Proteins were separated on 4 to 12% NuPAGE Bis-Tris polyacrylamide gels (Invitrogen WG1402), transferred to a nitrocellulose membrane, and probed with antibodies against LKB1 (Santa Cruz sc-374334), GAPDH (CST 2118S), phospho-AMPKα T172 (CST 2535S), AMPKα (CST 5832S), phospho-ULK1 S555 (CST 5869S), ULK1 (CST 8054S), phospho-MEK1/2 S217/221 (CST 9154S), MEK1/2 (CST 8727S), phospho-ERK1/2 T202/Y204 (CST 4370S), ERK1/2 (CST 4695S), phospho-AKT T308 (CST 4056S), AKT1 (CST 2938S), phospho-S6 S240/244 (CST 5364S), S6 (CST 2217S), β-actin (CST 3700S), FIG4 (Novus NBP3-05130), and VAC14 (Sigma-Aldrich SAB4200074).

For the measurements of phospho-EGFR Y1068 and total EGFR in spheroids, an Alpha SureFire Ultra Multiplex Phospho-EGFR (Tyr1068) and Total EGFR Assay Kit (PerkinElmer MPSU-PTEGFR-K-HV) was used. To perform these measurements, spheroids were lysed 72h after the addition of the methylcellulose-containing media. For each condition, 48 spheroids were pooled, rinsed once with PBS, and then resuspended in 100 μL RIPA buffer. Spheroids were then sonicated and subjected to one freeze-thaw cycle prior to performing the assay. Six measurements were performed for each condition. The signal intensity for phospho-EGFR Y1068 for each well was normalized to the total EGFR signal intensity from the same well.

CRISPR Screens. Genome-wide screens were performed with the TKOv3 CRISPR library (Addgene 90294, a gift from Jason Moffat, University of Toronto). Lentivirus was generated from the plasmid library using 293FT cells and Lipofectamine 3,000-based transfection, as described above. For each line (EV and WT), approximately 30% of 144×10^6 cells were infected with the TKOv3 library virus, to achieve an average 500-fold representation of the sgRNAs in each condition of the screen. Cells were then selected on puromycin for 5 d. Next, 35×10^6 cells were seeded into either 2D or mass spheroid culture. For the 2D screen, cells were seeded into HYPERFlasks (Corning 10030). For the spheroid screen, cells were first resuspended in 36 mL of normal media and then resuspended in 144 mL of media containing methylcellulose. The cell suspension was then distributed evenly over 245 mm^2 square assay dishes (Corning 431111). To passage the cells in mass spheroid culture, spheroids were spun at 800 × g for 10 min, washed with PBS, resuspended in Accutase (STEMCELL Technologies 07920), and allowed to incubate at room temperature for 10 min with gentle agitation. Cells were passaged every 3 d for 21 d, at which point genomic DNA was extracted from cells grown under each condition. sgRNA inserts were amplified with NEBNext High-Fidelity 2× PCR Master Mix (NEB M0541L). Samples were then pooled in equimolar concentrations, purified by gel electrophoresis, and sequenced with an Illumina HiSeq kit. Sequencing reads were trimmed and aligned to the TKOv3 library using Cutadapt and Bowtie. This alignment returned a table of raw reads, and the sgRNAs with less than 30 raw reads were excluded from further analysis. The raw reads were then analyzed with MAGeCK-MLE to obtain a beta-score for each gene (38). The pathway enrichment analysis was performed with the pathfindR program in the R software package. sgRNAs with a beta score of >0.5 in the spheroids with WT *LKB1* and <0.5 in the *LKB1*-null spheroids were used as the input into pathfindR.

Proteomics and Kinase Activity Analyses. To analyze the proteome and phosphoproteome of *LKB1*-null and -WT cells, cells were seeded into 2D or spheroid culture, with 5 replicates per condition. After 48 h in culture, protein lysates were prepared in RIPA buffer. Proteins were then precipitated, digested with trypsin, desalted, and labeled with a TMTpro 16plex Label Reagent Set (Thermo Scientific A44520). Small aliquots of each TMT-labeled sample were mixed and analyzed by liquid chromatography–mass spectrometry (LC–MS) to evaluate peptide labeling and sample ratios. Based on those results, the remaining samples were mixed at equal ratios. The mixed, TMT-labeled samples were fractionated by Reversed-Phase Liquid Chromatography (RPLC) into 12 fractions. Five percent of each fraction was used for expression profiling. The remaining 95% was enriched for phosphorylated peptides by using TiO2 beads. All samples were analyzed by LC–MS. The resulting data were searched against a protein database using MaxQuant software. These data were then processed and statistically analyzed using Perseus and R software. All samples were normalized to their median signal intensities to account for differences in sample loading. To account for changes in the total levels of proteins, the relative signal intensities of phosphopeptides in the phosphoproteomics datasets were subsequently normalized to the median signal intensities of the corresponding peptides in the total proteomics datasets. To identify phosphopeptides that varied in abundance between spheroid and 2D culture, the relative signal intensities in the spheroid phosphoproteomics datasets were normalized to the corresponding median signal intensities in the 2D phosphoproteomics datasets. The kinase activity analysis was performed by using the "Enrichment Analysis" option of the "Kinase Prediction" tool available at https://www.phosphosite.org/kinaseLibraryAction.

Kinase Prediction Analyses. The kinase prediction analyses for serine and threonine residues on the PIKFYVE complex and PTPN12 were performed by using the "Score Site" option of the Kinase Prediction tool (see URL above). The data from these predictions were further analyzed and visualized in R.

Measurement of Endocytosis. Measurement of EGFR internalization was performed by using pHrodo Red EGF (Invitrogen P35374) at a concentration of 0.5 μg/mL, pHrodo Red transferrin (Invitrogen P35376) at 25 μg/mL, and pHrodo Red dextran (Invitrogen P10361) at 20 μg/mL. pHrodo-linked substrates were added to spheroids 24 h after adding methylcellulose-containing media. The mean signal intensity for red fluorescence was measured with an Incucyte S3 and then normalized to the area of the spheroid.

Analysis of Human LUAD Sequencing Data. To assess the rates of occurrence of mutations in *LKB1* and *EGFR* and amplifications of *FGFR4*, *HER2*, and *MET*, the cBioPortal database was used to combine and analyze 3 studies of LUAD tumors (MSK, J Thoracic Oncology 2020; MSK, NPJ Precision Oncology 2021; MSK, 2021). Alterations of unknown significance were excluded from the analysis.

Statistical Analysis. Data were visualized, and statistical analyses were performed using GraphPad Prism 9 and R. $P < 0.05$ was considered statistically significant. To evaluate for statistically significant differences among groups in the xenograft and spheroid growth assays, the area under the curve (AUC) was first determined for each condition. Next, a two-tailed, unpaired *t* test was used to compare AUCs in experiments with two conditions. For experiments involving greater than two conditions, ANOVA was used to compare AUCs. Additionally, for experiments with greater than two conditions, the group corresponding to *LKB1*-WT (or *LKB1*-WT with sgCTRL, DMSO, or H_2O) was used as the reference. The Dunnett method was used to correct for multiple hypothesis testing. To evaluate for statistically significant differences among conditions in the proteomics experiments, *P*-values were calculated using the 2-sample *t* test, and the false discovery rate method was used to correct for multiple hypothesis testing. To evaluate for statistically significant differences among conditions in the LC3 degradation assays, the p-EGFR measurement assay, and the EGFR internalization assays, *P*-values were calculated by using a two-tailed, unpaired *t* test for experiments with two conditions. For experiments involving greater than two conditions, ANOVA was used to determine the *P*-value. The Tukey method was used to correct for multiple hypothesis testing. For statistical analysis of the human LUAD sequencing data, *P*-values were calculated by using a two-tailed Fisher's exact test.

Data, Materials, and Software Availability. The CRISPR screen and proteomics data have been deposited at Harvard Dataverse (39–41). Additionally, an open access license will be requested for this manuscript. All data are available in the manuscript or *SI Appendix*.

ACKNOWLEDGMENTS. We thank Guoan Zhang (Department of Biochemistry, Weill Cornell Medicine) and the Proteomics & Metabolomics Core Facility at Weill Cornell Medicine for assistance with the proteomics experiments, Wei Li (Departments of Genomics and Precision Medicine and Pediatrics, George Washington University) for providing guidance on the analysis of the CRISPR screens, Kyuho Han (MEDIC Life Sciences) for providing guidance on culturing spheroids, and Long He (Department of Pharmacology, Weill Cornell Medicine) and Timothy McGraw (Department of Biochemistry, Weill Cornell Medicine) for critical discussions of the data. This work was funded by the Lee Cooperman Physician-Scientist Training Award of the Damon Runyon Cancer Research Foundation DRG 18-18 (J.R.F.); Kenneth G. and Elaine A. Langone Fellow Award of the Damon Runyon Cancer Research Foundation DRG-2343-18 (E.E.G.); National Cancer Institute grant R35CA197588 (L.C.C.); and National Human Genome Research Institute grants R01CA218668, R01CA279135, DP2HG010099, and R00HG008171 (N.E.S.).

Author affiliations: [a]Meyer Cancer Center, Weill Cornell Medicine, New York, NY 10021; [b]Division of Hematology and Medical Oncology, Department of Medicine, Weill Cornell Medicine, New York, NY 10021; [c]Department of Pharmacology, Weill Cornell Medicine, New York, NY 10021; [d]New York Genome Center, New York, NY 10013; [e]Department of Biology, New York University, New York, NY 10003; and [f]Department of Medicine, Weill Cornell Medicine, New York, NY 10021

Author contributions: J.R.F., J.T., A.M.U., Y.Z., L.C.C., J.B., N.E.S., and H.V. designed research; J.R.F., J.T., Y.Z., M.J.N., E.E.G., O.M., K.L., N.K., A.M., and M.M. performed research; J.R.F. contributed new reagents/analytic tools; J.R.F., J.T., A.M.U., Y.Z., M.J.N., L.C.C., J.B., N.E.S., and H.V. analyzed data; and J.R.F. and H.V. wrote the paper.

1. D. B. Shackelford, R. J. Shaw, The LKB1–AMPK pathway: Metabolism and growth control in tumour suppression. *Nat. Rev. Cancer* **9**, 563–575 (2009), 10.1038/nrc2676.
2. N. Krishnamurthy, A. M. Goodman, D. A. Barkauskas, R. Kurzrock, STK11 alterations in the pan-cancer setting: Prognostic and therapeutic implications. *Eur. J. Cancer* **148**, 215–229 (2021), 10.1016/j.ejca.2021.01.050.
3. P. E. Hollstein *et al.*, The AMPK-related kinases SIK1 and SIK3 mediate key tumor-suppressive effects of LKB1 in NSCLC. *Cancer Discov.* **9**, 1606–1627 (2019), 10.1158/2159-8290.CD-18-1261.
4. C. W. Murray *et al.*, An LKB1-SIK axis suppresses lung tumor growth and controls differentiation. *Cancer Discov.* **9**, 1590–1605 (2019), 10.1158/2159-8290.CD-18-1237.
5. H. Mehenni *et al.*, Loss of LKB1 kinase activity in Peutz-Jeghers syndrome, and evidence for allelic and locus heterogeneity. *Am. J. Hum. Genet.* **63**, 1641–1650 (1998), 10.1086/302159.
6. T. B. Sundberg *et al.*, Development of chemical probes for investigation of salt-inducible kinase function in vivo. *ACS Chem. Biol.* **11**, 2105–2111 (2016), 10.1021/acschembio.6b00217.
7. K. H. Vining, D. J. Mooney, Mechanical forces direct stem cell behaviour in development and regeneration. *Nat. Rev. Mol. Cell Biol.* **18**, 728–742 (2017), 10.1038/nrm.2017.108.
8. J. L. Johnson *et al.*, An atlas of substrate specificities for the human serine/threonine kinome. *Nature* **613**, 759–766 (2023), 10.1038/s41586-022-05575-3.
9. M. Martini, M. C. De Santis, L. Braccini, F. Gulluni, E. Hirsch, PI3K/AKT signaling pathway and cancer: An updated review. *Ann. Med.* **46**, 372–383 (2014), 10.3109/07853890.2014.912836.
10. T. Hart *et al.*, Evaluation and design of genome-wide CRISPR/SpCas9 knockout screens. *G3 (Bethesda)* **7**, 2719–2727 (2017), 10.1534/g3.117.041277.
11. J. A. Lees, P. Li, N. Kumar, L. S. Weisman, K. M. Reinisch, Insights into lysosomal PI(3,5)P2 homeostasis from a structural-biochemical analysis of the PIKfyve lipid kinase complex. *Mol. Cell* **80**, 736–743.e4 (2020), 10.1016/j.molcel.2020.10.003.
12. M. Mohseni *et al.*, A genetic screen identifies an LKB1-MARK signalling axis controlling the Hippo-YAP pathway. *Nat. Cell Biol.* **16**, 108–117 (2014), 10.1038/ncb2884.
13. J. E. Duex, J. J. Nau, E. J. Kauffman, L. S. Weisman, Phosphoinositide 5-phosphatase Fig 4p is required for both acute rise and subsequent fall in stress-induced phosphatidylinositol 3,5-bisphosphate levels. *Eukaryot. Cell* **5**, 723–731 (2006), 10.1128/EC.5.4.723-731.2006.
14. J. E. Duex, F. Tang, L. S. Weisman, The Vac14p-Fig4p complex acts independently of Vac7p and couples PI3,5P2 synthesis and turnover. *J. Cell Biol.* **172**, 693–704 (2006), 10.1083/jcb.200512105.
15. N. Jin *et al.*, VAC14 nucleates a protein complex essential for the acute interconversion of PI3P and PI(3,5)P(2) in yeast and mouse. *EMBO J.* **27**, 3221–3234 (2008), 10.1038/emboj.2008.248.
16. A. Shisheva, PIKfyve: The road to PtdIns 5-P and PtdIns 3,5-P(2). *Cell Biol. Int.* **25**, 1201–1206 (2001), 10.1006/cbir.2001.0803.
17. Y. Posor, W. Jang, V. Haucke, Phosphoinositides as membrane organizers. *Nat. Rev. Mol. Cell Biol.* **23**, 797–816 (2022), 10.1038/s41580-022-00490-x.
18. X. Cai *et al.*, PIKfyve, a class III PI kinase, is the target of the small molecular IL-12/IL-23 inhibitor apilimod and a player in Toll-like receptor signaling. *Chem. Biol.* **20**, 912–921 (2013), 10.1016/j.chembiol.2013.05.010.
19. S. Gayle *et al.*, Identification of apilimod as a first-in-class PIKfyve kinase inhibitor for treatment of B-cell non-Hodgkin lymphoma. *Blood* **129**, 1768–1778 (2017), 10.1182/blood-2016-09-736892.
20. Cancer Genome Atlas Research Network, Comprehensive molecular profiling of lung adenocarcinoma. *Nature* **511**, 543–550 (2014), 10.1038/nature13385.
21. Y. Liu *et al.*, Phosphatidylinositol 3-phosphate 5-kinase (PIKfyve) is an AMPK target participating in contraction-stimulated glucose uptake in skeletal muscle. *Biochem. J.* **455**, 195–206 (2013), 10.1042/BJ20130644.
22. J. de Lartigue *et al.*, PIKfyve regulation of endosome-linked pathways. *Traffic* **10**, 883–893 (2009), 10.1111/j.1600-0854.2009.00915.x.
23. E. E. Er, M. C. Mendoza, A. M. Mackey, L. E. Rameh, J. Blenis, AKT facilitates EGFR trafficking and degradation by phosphorylating and activating PIKfyve. *Sci. Signal* **6**, ra45 (2013), 10.1126/scisignal.2004015.
24. F. A. Suprynowicz *et al.*, The human papillomavirus type 16 E5 oncoprotein inhibits epidermal growth factor trafficking independently of endosome acidification. *J. Virol.* **84**, 10619–10629 (2010), 10.1128/JVI.00831-10.
25. Y. Liu *et al.*, Metabolic and functional genomic studies identify deoxythymidylate kinase as a target in LKB1-mutant lung cancer. *Cancer Discov.* **3**, 870–879 (2013), 10.1158/2159-8290.CD-13-0015.
26. H. Varmus, A. M. Unni, W. W. Lockwood, How cancer genomics drives cancer biology: Does synthetic lethality explain mutually exclusive oncogenic mutations? *Cold Spring Harb. Symp. Quant. Biol.* 81, 247–255 (2016), 10.1101/sqb.2016.81.030866.
27. E. Cerami *et al.*, The cBio cancer genomics portal: An open platform for exploring multidimensional cancer genomics data. *Cancer Discov.* **2**, 401–404 (2012), 10.1158/2159-8290.CD-12-0095.
28. I. S. Okon, K. A. Coughlan, M. H. Zou, Liver kinase B1 expression promotes phosphatase activity and abrogation of receptor tyrosine kinase phosphorylation in human cancer cells. *J. Biol. Chem.* **289**, 1639–1648 (2014), 10.1074/jbc.M113.500934.
29. M. P. Patricelli *et al.*, Selective inhibition of oncogenic KRAS output with small molecules targeting the inactive state. *Cancer Discov.* **6**, 316–329 (2016), 10.1158/2159-8290.CD-15-1105.
30. P. Lito, M. Solomon, L. S. Li, R. Hansen, N. Rosen, Allele-specific inhibitors inactivate mutant KRAS G12C by a trapping mechanism. *Science* **351**, 604–608 (2016), 10.1126/science.aad6204.
31. X. Wang *et al.*, Identification of MRTX1133, a noncovalent, potent, and selective KRAS(G12D) inhibitor. *J. Med. Chem.* **65**, 3123–3133 (2022), 10.1021/acs.jmedchem.1c01688.
32. S. Zheng *et al.*, SynergyFinder plus: Toward better interpretation and annotation of drug combination screening datasets. *Genom. Proteom. Bioinform.* **20**, 587–596 (2022), 10.1016/j.gpb.2022.01.004.
33. B. D. Stein *et al.*, LKB1-dependent regulation of TPI1 creates a divergent metabolic liability between human and mouse lung adenocarcinoma. *Cancer Discov.* **13**, 1002–1025 (2023), 10.1158/2159-8290.CD-22-0805.
34. A. Tomas, C. E. Futter, E. R. Eden, EGF receptor trafficking: Consequences for signaling and cancer. *Trends Cell Biol.* **24**, 26–34 (2014), 10.1016/j.tcb.2013.11.002.
35. M. Gao *et al.*, SPRY2 loss enhances ErbB trafficking and PI3K/AKT signalling to drive human and mouse prostate carcinogenesis. *EMBO Mol. Med.* **4**, 776–790 (2012), 10.1002/emmm.201100944.
36. L. J. Eichner *et al.*, Genetic analysis reveals AMPK is required to support tumor growth in murine kras-dependent lung cancer models. *Cell Metab.* **29**, 285–302.e7 (2019), 10.1016/j.cmet.2018.10.005.
37. K. Han *et al.*, CRISPR screens in cancer spheroids identify 3D growth-specific vulnerabilities. *Nature* **580**, 136–141 (2020), 10.1038/s41586-020-2099-x.
38. B. Wang *et al.*, Integrative analysis of pooled CRISPR genetic screens using MAGeCKFlute. *Nat. Protoc.* **14**, 756–780 (2019), 10.1038/s41596-018-0113-7.
39. J. Ferrarone, "Proteomics in LKB1-null and -WT cells in spheroid culture". Harvard Dataverse, V1. https://doi.org/10.7910/DVN/DIYFCX. Deposited 2 May 2024.
40. J. Ferrarone, "Proteomics in LKB1-null and -WT cells in 2D culture". Harvard Dataverse, V1. https://doi.org/10.7910/DVN/HYFUFM. Deposited 2 May 2024.
41. J. Ferrarone, "CRISPR screens in LKB1-null and -WT cells". Harvard Dataverse, V1. https://doi.org/10.7910/DVN/8DEPIT. Deposited 2 May 2024.